

International Journal of Nanoelectronics and Materials

MosVCI

ISSN 1985-5761 | E-ISSN 2232-1535



Comparative study of graphene and reduced graphene oxide: synthesis, characterization, and electrical conductivity

Mohamed K. Fathy a *, Ahmed H. Zaki a, and Heba A. Shawkey b

- ^aMilitary Technical College, Elkobbah bridge, Cairo, 11772, Egypt
- ^bElectronic Research Institute, Huckstep, Cairo, 11773, Egypt
- *Corresponding author. Tel.: +01011143689; fax: +2-02-2262-1908; e-mail: muhammadkhaled@mtc.edu.eg

Received 13 May 2024, Revised 13 May 2025, Accepted 01 July 2025

ABSTRACT

A lot of interest has been focused on carbon allotropes, especially graphene and reduced graphene oxide. This is due to their outstanding electrical and mechanical properties, which enable their use in many electronic applications. In this work, graphene and reduced graphene oxide (RGO) samples were prepared by different techniques. Graphene was prepared by a physical sputtering method, whereas RGO was prepared by the improved Hummer's chemical method followed by chemical reduction. The prepared samples were characterized using Raman, X-ray diffraction, and energy-dispersive X-ray spectroscopy techniques. The graphene and RGO samples were qualified and compared to similar published works. A comparable quality factor value as high as 0.63 was obtained for the graphene compared to 0.09 for the RGO. The electrical conductivity of both graphene and RGO samples was also calculated from the I–V curves. A relatively high electrical conductivity of 153 S/cm was obtained for the graphene sample compared to 1.3×10^{-4} S/cm for the RGO sample. Graphene thin film shows higher electric conductivity relative to RGO thin film, which is in agreement with the proposed quality factor results.

Keywords: Graphene, Reduced graphene oxide, Sputtering, Quality factor, Electric conductivity

1. INTRODUCTION

Carbon is one of the most significant elements that has made significant contributions to nanomaterial technology. Graphite and its derived carbon family, including graphene, graphene oxide, and reduced graphene oxide, are carbon allotropes that have attracted growing curiosity from the field of science since Andre Geim and Konstantin Novoselov won the 2010 Nobel Prize. This increasing interest is due to their validity for many electronic applications such as electrodes, sensors, supercapacitors, and batteries [1, 2]. Graphite consists of stacked layer sheets of hybridized carbon atoms bonded to each other in a crystalline structure. Graphene is a mono- or few-layer of graphite atoms bonded in Sp2 hybridization form and arranged in a hexagonal shape. Recently, many graphene synthesis methods have been developed concerning the quality of the produced samples, low cost, simplicity, and validity for mass production [3]. Bottom-up and top-down approaches are the common techniques used generally for graphene preparation. The bottom-up approach is mainly dependent on the formation of graphene layer(s) from hydrocarbon sources under specific pressure and temperature conditions. It includes epitaxial graphene growth techniques such as sputtering [4, 5], chemical vapor deposition (CVD) [6], plasma-enhanced chemical vapor deposition (PECVD) [7]. However, these techniques are expensive and not simple. On the other hand, the top-down approach relies on oxidation, exfoliation, reduction, and

other chemical processes to break down the carbon material source into nanoscale compounds [5, 8, 9]. The main advantage of this approach is that it is simple, low-cost, and suitable for mass production [10]. This work aims to prepare graphene by both approaches and make a comparative study between the obtained products concerning the quality and the electrical conductivity points of view. In this work, graphene and reduced graphene oxide (RGO) are prepared physically by a bottom-up approach and chemically by a top-down approach, respectively. The prepared samples were characterized using Raman spectroscopy, X-ray diffraction (XRD), and scanning electron microscopy (SEM). The quality and electric conductivity of both samples were investigated and compared to other published works.

2. EXPERIMENTAL WORK

Graphene and RGO powder were prepared by physical and chemical methods, respectively.

2.1. Chemical Preparation of RGO

RGO thin film was synthesized on the top of a silicon wafer as a thin conductive film. A schematic diagram of the RGO thin film preparation process is shown in Figure 1. First, 10 grams of graphite powder (Techno PharmChem (TPC)) were added to 135 ml of concentrated orthophosphoric acid and 1200 ml of sulfuric acid. Then, 70 grams of potassium

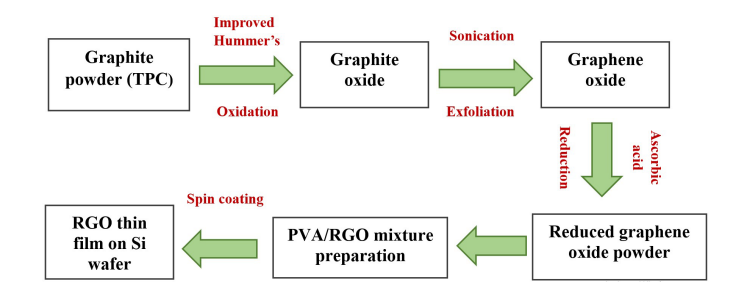


Figure 1. Schematic diagram of RGO thin film preparation

permanganate were gradually added to the mixture with careful stirring, and the mixture was kept at room temperature till it became homogeneous to form graphite oxide. This was followed by adding 100 ml of hydrogen peroxide (H2O2) and distilled water to the mixture with careful stirring, and a brown to yellowish color was observed, indicating the formation of graphene. The GO sample was chemically reduced using 8 grams of ascorbic acid to give RGO. The sample was filtered through filter paper and dried in an oven at a temperature of 60-75°C till obtaining RGO powder. For RGO/PVA mixture preparation, the silicon wafer was pre-cleaned in acetone and distilled water and then placed in a UV ozone cleaner to clean its surface. A polyvinyl alcohol (PVA) solution was prepared by mixing 500 mg of PVA powder with 10 ml of distilled water. The mixture was stirred on a magnetic stirrer at 55°C till it became a homogeneous solution. The RGO solution was formed by mixing the RGO powder with distilled water, followed by a sonication process. This RGO solution was carefully added to the PVA solution and stirred till it gave a homogeneous RGO/PVA solution that was spin-coated on a silicon wafer to form an RGO thin film. Finally, the wafer was heated in a drying oven at 180°C.

2.2. Physical Preparation of Graphene

This technique depends on depositing a rich film of carbon, such as silicon carbide (SiC), onto a metal film, such as nickel (Ni), which adsorbs the silicon from the silicon carbide film, forming metal silicide in a high-temperature environment through the annealing process. Ni reacts with SiC upon heating the Si/SiC/Ni structure, resulting in a mixture of Ni silicide and a carbon layer. As a result, carbon atoms diffuse into the Ni layer and aggregate on the Ni surface since carbon is poorly soluble in Ni [11]. Due to the low graphitization temperature of carbon on Ni surfaces, graphene is formed on the surface of the Ni silicide. So, the annealing process of the Si/SiC/Ni structure causes graphene to accumulate at the top of the Ni layer and the creation of a carbon-rich layer on top of the Ni-SiC surface interface. A 4" sputtering system model (Denton Vacuum Desktop Pro) was used for sputtering silicon carbide and nickel films on top of silicon wafers using SiC and Ni targets. A tube furnace was used for the annealing process of the sample. A schematic diagram of graphene thin film preparation is shown in Figure 2. First, the Si wafer was cleaned in a UV ozone cleaner (Ossila model) with isopropyl alcohol to be ready for the sputtering process. A 450 nm SiC film was deposited on the Si wafer using an RF power supply and an argon flow rate of 30 sccm for 1 hour. Then, a

50 nm thin Ni film was RF sputtered onto the Si/SiC stack in the presence of argon gas to form a Si/SiC/Ni structure. Ni is used as a catalytic metal to reduce the annealing time required for graphene growth at growth temperatures around 900-1100°C [12]. Many other metals can be used as catalysts for graphene formation, such as Cu [13, 14] and platinum [15]. Compared to Ni, platinum is more expensive than Ni. However, concerning carbon atom diffusion, the diffusion of carbon atoms in nickel to form graphene is faster than that in copper [16]. Because of the limited carbon solubility in nickel, this facilitates the segregation of carbon atoms on the Ni surface during the cooling process, leading to the formation of graphene on the Ni/SiC interface [12]. The Si/SiC/Ni stack was placed in the tube furnace to be annealed at high temperatures. The furnace was heated gradually till it reached a temperature of 715°C with a heating rate of 8°C/min. The furnace temperature was kept constant at 715°C for 10 mins before it was cooled down to 150°C with a cooling rate of 12.5°C/min. Finally, the sample was etched using hydrochloric acid (HCl) to remove the Nisilicide layer formed during the annealing process. This etching process was followed by rinsing in distilled water. Techniques based on graphene growth on SiC substrates at low temperatures in the presence of metal catalysts are very promising methods to obtain graphene [17]. However, the annealing time, annealing temperatures, and the degree of solubility of carbon in catalytic metals affect the quality of the obtained graphene [18].

3. SAMPLE CHARACTERIZATION

Several characterization techniques were used to examine the morphological, structural, and electrical properties of graphene and RGO samples. A Horiba Lab Ram HR EV (HR800) model Raman spectrometer with a 10-mW power supply and a 1000–3500 cm⁻¹ scan range was employed for sample characterization. In addition, a Bruker D8 Advance model X-ray diffractometer (40 kV X-ray, wavelength $\lambda = 1.54$ Å) was employed to determine the interlayer spacing and diffraction angle of the graphitic samples. An energy-dispersive X-ray spectroscopy (EDX) system equipped with a ZEISS EVO 40SE detector was also used to scan the materials' surfaces and analyze the composition of the formed graphene and RGO layers. To study the electric characteristics of graphene and RGO samples, the I-V characteristics of the prepared samples were measured using a Keithley 4200 SCS model with a scan voltage range of -5V to +5V. This was used to calculate the electric conductivity of the prepared samples.

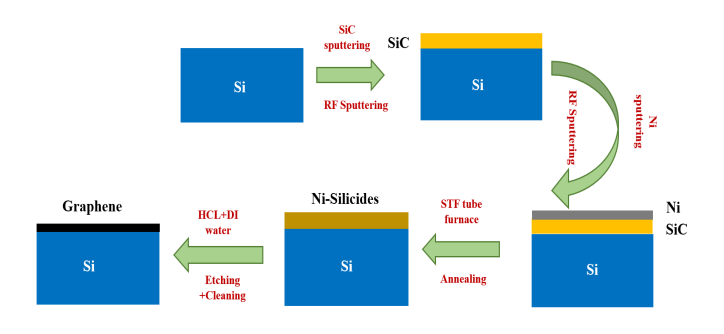


Figure 2. Schematic drawing of graphene thin film preparation

4. DISCUSSIONS AND RESULTS

This section provides detailed information about the characterization results of the prepared graphene and RGO samples by physical and chemical methods.

4.1. Raman Spectroscopy

Raman spectroscopy is usually used to give information about the stacking order and the structural defects of graphene. Raman spectra give a molecular fingerprint, as different molecules have different Raman spectra. It can also be used for qualitative and quantitative analysis [19, 20]. The measured Raman spectra for both RGO and graphene samples are shown in Figure 3. Three main Raman peaks appeared at (1345 cm⁻¹), (1566 cm⁻¹) and (2698 cm⁻¹) for RGO and (1270 cm⁻¹), (1571 cm⁻¹) and (2756 cm⁻¹) for graphene, which correspond to the D, G, and 2D bands, respectively. "G-peak" reflects the in-plane vibrations caused by the sp² hybridization of carbon atoms [21, 22]. "D-peak" describes sp3 disorder and sp2 lattice defects [20-22]. The number of graphene layers is represented by a "2D peak", which is the second order of the D-band caused by the two-phonon lattice vibration process [22-25]. Concerning the ratios between Raman peaks, as the intensity ratio I_D/I_G is lower, it corresponds to fewer structural disorders in the graphitic structure, as well as a higher carbon-to-oxygen ratio, which means an increase in the graphitic carbon structure [26, 27]. The number of graphene layers is shown to be inversely proportional to the I_{2D}/I_G ratio [28, 29]. As this ratio increases, the number of graphene layers decreases. It's been noticed that the ID/IG

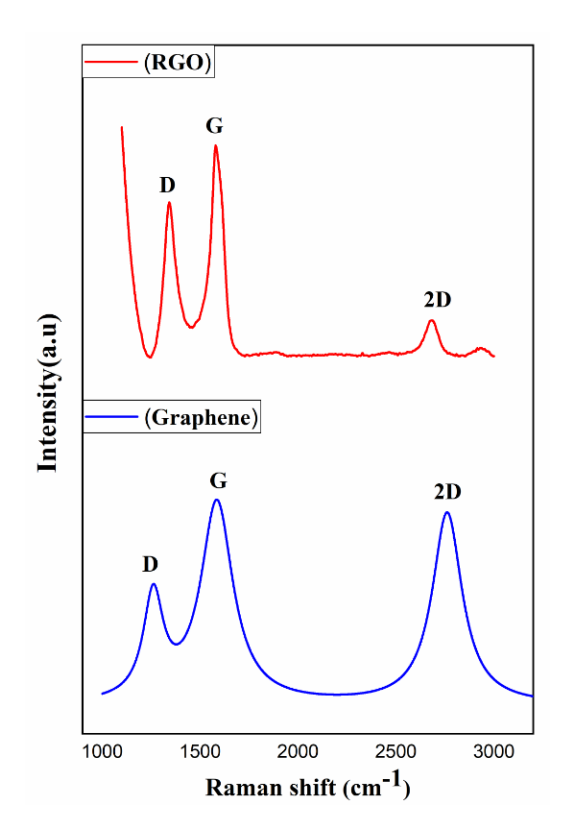


Figure 3. Raman spectra of RGO and graphene samples

ratio for the RGO sample is higher than that of the graphene sample, which means that RGO has larger structure defects and sp³ disorders than graphene. This is attributed to the use of chemical agents during RGO preparation as oxidizing and reducing agents that cause many defects in the formed RGO sheets, whereas physically prepared graphene isn't subjected to any chemical agents during preparation. The ratio of I_{2D}/I_G appeared to be higher in the graphene sample than in the RGO sample, which means that the number of graphene layers was lower, indicating a higher quality in the graphene sample than the RGO sample. Table 1 indicates a comparative study for calculated peak ratios for both RGO and graphene samples. Generally, it can be observed that the quality of the graphene is higher than that of the RGO. In addition, Raman shots were taken to examine the film surfaces of both graphene and RGO samples, as shown in Figure 4. Raman imaging of graphene shows some pores on its surface, as shown in Figures 4a and b. Porous areas that appear as grey-colored areas are graphene-free areas (Siwafer) due to the excess etching process in these regions, whereas a yellow-colored surface indicates grapheneformed regions on the silicon wafer. Figures 4c and d show Raman images of RGO thin film. It appears as a homogeneous continuous layer of reduced graphene oxide film.

4.2. X-Ray Diffraction (XRD)

XRD is usually used for the characterization of carbon nanomaterial structures. The interlayer spacing and crystal size of the prepared samples were determined by XRD characterization based on the position and the broadness of

Table 1. Ratio of Raman peaks intensity for graphene and RGO samples

Sample	I _D /I _G	I_{2D}/I_{G}	I_{2D}/I_{D}
Graphene	0.58	0.94	1.61
RGO	0.73	0.17	0.23

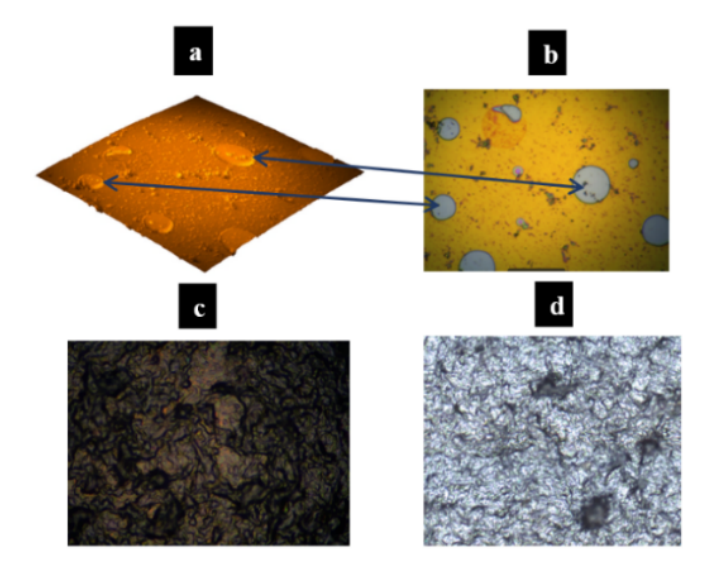


Figure 4. Raman imaging of (a, b) graphene and (c, d) RGO surfaces

the XRD peak. According to Bragg's rule, the interlayer spacing (d spacing) between graphene/RGO sheets increases as the position of 2θ decreases as follows:

$$n\lambda = 2d\sin\theta \tag{1}$$

where n is an integer representing the order of the diffraction peak and λ is the X-ray wavelength. In the XRD pattern shown in Figure 5, a sharp and intense peak was observed for graphite at $2\theta=26.6^{\circ}$, corresponding to the (002) diffraction plane with a lattice spacing of 0.34 nm [30–32]. This peak is characteristic of the crystalline structure of pure graphite. Upon oxidation and exfoliation of graphite to form graphene oxide (GO), the introduction of oxygen-containing functional groups between the graphite layers led to an increase in interlayer spacing, appearing as a shifting of the (002) peak to $2\theta=10.9^{\circ}$, corresponding to a d-spacing of 0.81 nm. This confirms the successful formation of GO with expanded layer separation.

For the RGO sample, a broad and low-intensity peak appears at $2\theta = 23.5^{\circ}$, corresponding to an interlayer spacing of 0.38 nm. This broadening and intensity reduction indicate the presence of small, disordered crystallites, typically resulting from the reduction of GO. The removal of oxygenated functional groups during the reduction process causes the re-aggregation of graphene layers via van der Waals forces [33, 34], as reflected in the shift of the diffraction peak from 10.9° back to 23.5°, confirming partial restoration of the sp²-hybridized graphitic structure. Figure 6 compares the XRD patterns of graphene with that of RGO. The graphene sample exhibits a sharp peak at 2θ = 23.1°, with a corresponding d-spacing of 0.39 nm, indicating partial exfoliation and higher crystallinity relative to RGO. The sharpness and intensity of this peak suggest the formation of larger crystallites after thermal annealing. In contrast, the RGO pattern again shows the broader (002) peak at $2\theta = 23.5^{\circ}$, reflecting a lower degree of crystallinity. For graphene, the crystallographic orientation of the film after the annealing process was examined. Table 2 summarizes the measured 2θ values and calculated interlayer spacings for both graphene and RGO. The differences in peak sharpness further support the crystallite size interpretation: sharp peaks correspond to larger, more ordered domains, while broader peaks indicate smaller crystallites [35]. Thus, the XRD analysis confirms that the graphene sample exhibits higher structural order than RGO.

Concerning the average crystallite size of the prepared samples, the most commonly used method to estimate the average crystallite size is using the Scherrer equation. The Scherrer equation relates the average crystallite size (D) to the peak broadening (β) observed in the XRD pattern, the X-ray wavelength (λ), and the Bragg angle (θ). The equation is as follows:

$$D = \frac{\kappa \lambda}{\theta \cos(\theta)} \tag{2}$$

where D is the average crystallite size, K is the Scherrer constant, λ is the X-ray wavelength, β is the full width at half

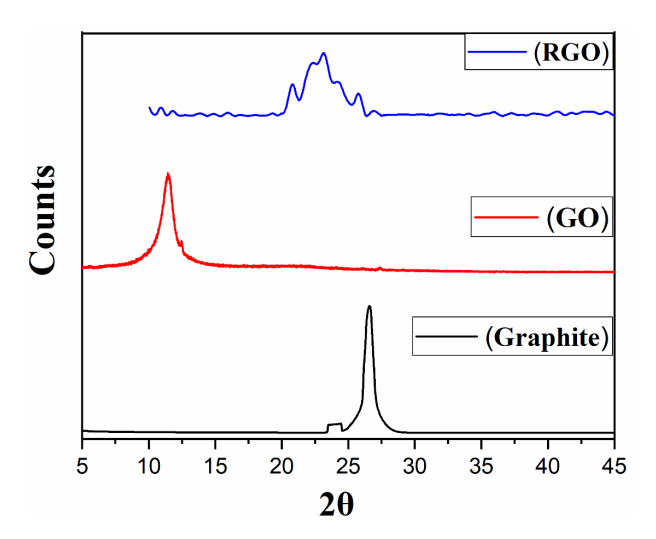


Figure 5. XRD analysis of graphite, GO, and RGO samples

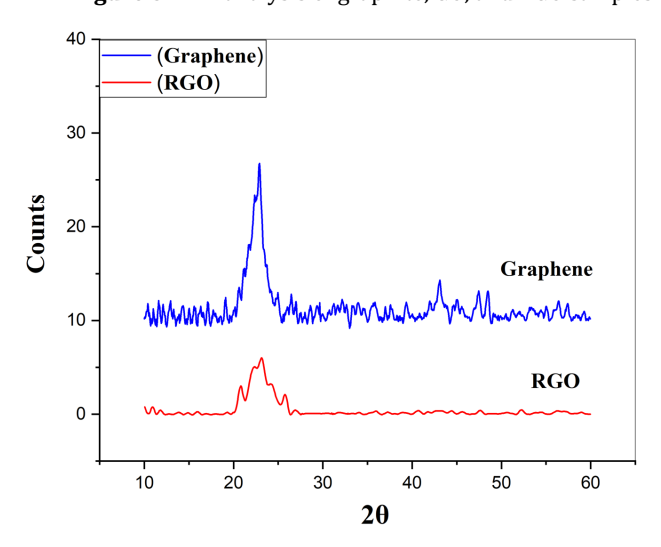


Figure 6. XRD analysis of graphene and RGO powder samples

maximum (FWHM) of the XRD peak, and θ is the Bragg angle. The FWHM of the XRD peak of all graphitic samples, the position of 2θ (Bragg angle), and the factors of XRD patterns fitting were obtained after fitting all graphitic curves using the Origin Pro software (2018 64-bit). The average crystallite size was calculated for graphene and RGO samples using Scherrer equation and it was found equal to 4.17 nm and 2.53 nm for graphene and RGO, respectively as shown in Table 3.

Table 2. Position of 2θ of graphene and RGO samples and their corresponding interlayer spacing

Powder	2θ	d (nm)
Graphene	23.1°	0.39
RGO	23.5°	0.38

Table 3. Average crystallite size of graphene and RGO samples

Sample	X-ray wavelength (λ)	Peak position (2θ)	FWHM (ß) radians	Crystal size D (nm)
Graphene	0.154	23.1°	1.944	4.17
RGO	0.154	23.5°	3.200	2.53

4.3. Energy-Dispersive X-ray Spectroscopy (EDX)

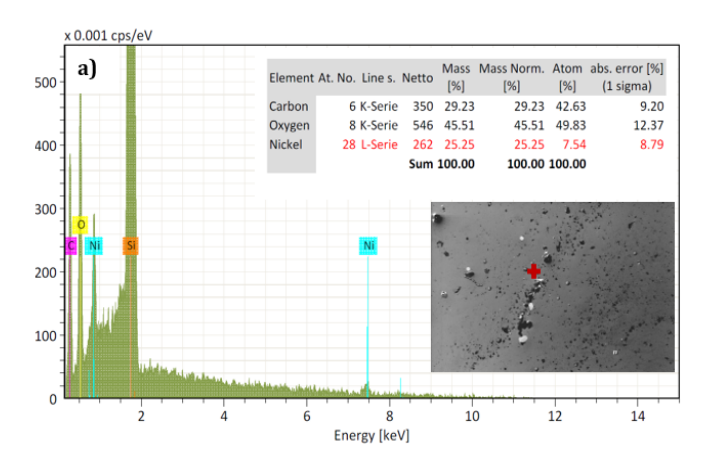
Energy dispersive X-ray analysis (EDX) was used to analyze the composition of graphene and RGO films. The formed graphene layer before and after the etching process was investigated, as shown in Figure 7. Before the etching process, the Ni mass percentage in the sample was 25.25% compared to the carbon mass percentage of 29.23% as shown in Figure 7a. However, the Ni mass percentage was reduced to 2.46% compared to the carbon mass percentage of 35.12% after the etching process. There was a noticeable increase in carbon net mass in the sample (from 29.23% to 35.12%) compared to a noticeable decrease in Ni net mass from 25.25% to 2.46%, as shown in Figure 7b. This confirms the removal of Ni-silicides from the surface and the formation of a rich carbon layer. Energy dispersive X-ray analysis (EDX) was also used to analyze the composition of the RGO thin film, as shown in Figure 8. EDX analysis confirms the presence of carbon and oxygen in the RGO structure. However, the carbon percentage was greater than that of oxygen in the RGO structure, which confirms the successful reduction of graphene oxide into RGO, the removal of the majority of the oxygenated functional groups, and the restoration of the graphitic structure after the chemical treatment using the oxidizing and reducing agents.

5. QUALIFICATION

In our previous work [3], a new quality factor was proposed for qualifying the prepared graphene, which can be derived from XRD and Raman measurements. Equation (3) yields the suggested quality factor (Q) as:

$$Q = d \times \frac{I_{2D}}{I_D} \tag{3}$$

where d is the interlayer spacing between layers as determined by XRD analysis calculations and I2D/ID is the intensity ratio of the Raman spectra for the 2D and D peaks, respectively. It is clear from the prior conclusions that highquality graphene is dependent on a higher carbon content with minimum structural defects and the largest layer spacing between graphene layers. This corresponds to obtaining both the least (I_D/I_G) and the greatest (I_{2D}/I_G) ratios. Stated differently, it is about getting the maximum ratio of (I_{2D}/I_D). Higher quality factor values indicate a higher-quality final product. Table 4 shows a comparative study comparing the extracted quality factor of our chemically prepared RGO and physically prepared graphene thin films, respectively, along with the corresponding literature published reports. Generally, it can be noticed that the quality factor (Q) of bottom-up approaches has higher values compared to that of top-down prepared approaches. This can be attributed to the advantage of using physical preparation methods instead of chemical methods. The problem with using chemical methods is the use of oxidizing and reducing agents during sample preparation. This led to many structural defects in the prepared samples, so the Raman intensity ratio of ID/IG appeared to be high. On the other hand, no chemical agents were used in the physical methods, so fewer imperfections



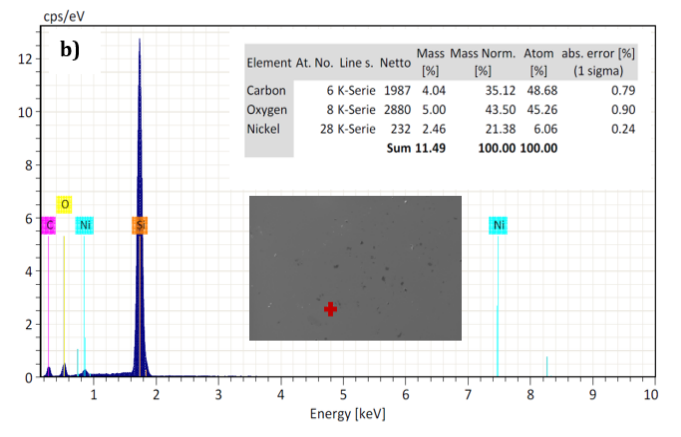


Figure 7. EDX analysis of graphene thin film (a) before and (b) after etching process

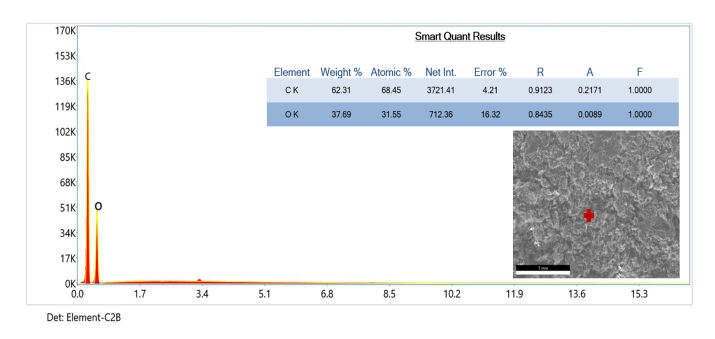


Figure 8. EDX analysis of the reduced graphene oxide

appeared in the prepared samples, corresponding to a lower I_D/I_G ratio, and consequently, higher Q values can be obtained.

6. ELECTRICAL CONDUCTIVITY MEASUREMENTS

The I–V measurements were analyzed for both graphene and RGO thin films. To fabricate the RGO film, RGO powder was re-dispersed in distilled water to form a homogeneous paste, which was spin-coated multiple times onto a silicon/silicon dioxide (Si/SiO₂) substrate. The structure was then thermally treated to produce a uniform and continuous RGO layer. For both graphene and RGO films, silver electrodes were deposited with electrode spacing (L) of 1.1 cm. The entire structure was subsequently annealed for 45 minutes to enhance contact quality and ensure complete drying, as shown in Figure 9. The thickness (t) of

Synthesis approach	Sample	I _D /I _G	I _{2D} /I _G	I_{2D}/I_{D}	2θ	d	Q	References
	Graphene thin film by sputtering	0.58	0.94	1.61	23.1	0.39	0.63	This work
	Courbons this film her CVD	0.85	2.407	2.82	26.6	0.33	0.93	[6]
	Graphene thin film by CVD	0.91	2.393	2.633	26.1	0.35	0.93	[6]
Bottom-up	RGO thin film by laser pulse deposition	1.653	0.133	0.08	15.9	0.55	0.04	
,		0.97	0.121	0.124	19.4	0.45	0.05	[36]
		1.57	0.251	0.16	16.2	0.54	0.08	
		1.14	0.171	0.15	15.8	0.56	0.08	
	RGO thin film by PVA	0.73	0.17	0.23	23.5	0.38	0.09	This work
	Graphene thin film by pyrolysis	0.636	0.136	0.214	26.4	0.34	0.07	[27]
	N-doped graphene thin film by pyrolysis	0.91	0.1186	0.129	26.4	0.34	0.04	[37]
Top-down	N-doped RGO thin film	0.87	0.06	0.07	24.6	0.36	0.02	[00]
	N-doped RGO thin film	0.855	0.068	0.08	25.5	0.35	0.02	[38]

0.265

1.07

0.457

0.141

1.724

0.132

Table 4. Extracted quality factor for some published works by bottom-up and top-down approaches

each film was measured using a KLA Tencor Alpha-Step D-500 stylus profiler. The graphene film exhibited a thickness of approximately 138 nm, while the RGO film reached 185.8 µm. Electrical characterization was performed using a two-point Keithley probe station (model SCS-4200) under ambient conditions at room temperature. As shown in Figure 10, I-V characteristics were recorded on both logarithmic and linear scales by sweeping the voltage from -3 V to +3 V. Electrical conductivity (σ) was calculated for both films using the relation:

Graphene-based thin film

RGO thin film

$$\sigma = L/_{R \times W \times t} \tag{4}$$

where R is the resistance extracted from the linear portion of the I-V curve, and L, W, and t represent the electrode spacing, electrode width, and film thickness, respectively. The extracted conductivity values are presented in Table 5 and compared with those reported in similar studies. The results demonstrate that graphene exhibits significantly higher electrical conductivity than RGO. This is attributed to the difference in synthesis approach, where the bottom-up method used for graphene results in fewer structural defects and improved sp2 bonding. In contrast, RGO, synthesized via a top-down chemical route involving strong oxidizing and reducing agents, retains a high density of sp³ defects, which significantly limit its electrical performance.

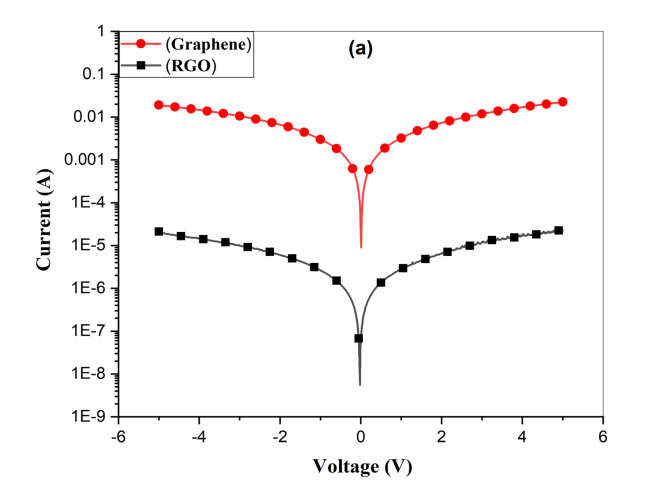


Table 5. The electric conductivity of graphene and RGO thin films

23.4

25.8

0.38

0.34

0.65

0.04

[39]

[40]

Synthesis Technique	Sample	Conductivity (S/cm)	Reference		
	Graphene	153	This work		
	Graphene / Epitaxial SiC	234	[41]		
Bottom-up	Graphene nanocomposite film	1.89	[42]		
	VGNS / CU foam	4.81×10^4	[7]		
	RGO-thin film	1.30×10^{-4}	This work		
Top-down	RGO-thin film	4.21 × 10 ⁻⁵	[43]		
	RGO-thin film	6.56 × 10 ⁻⁴	[44]		

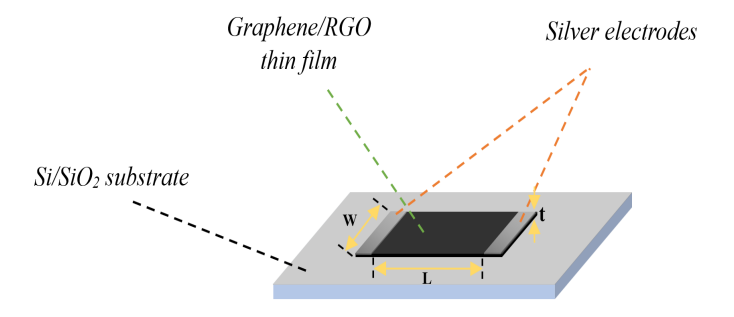


Figure 9. Schematic illustration of the I-V measurement setup for graphene and RGO thin films

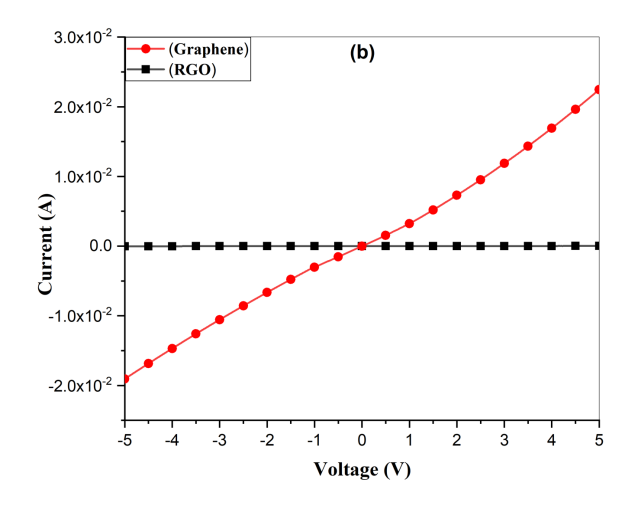


Figure 10. I-V characteristic curves of graphene and RGO thin films on (a) semi-log and (b) linear scales

7. CONCLUSION

Graphene and reduced graphene oxide thin films were prepared by physical (bottom-up) and chemical (top-down) preparation techniques respectively. Graphene was prepared by deposition of SiC and Ni films followed by annealing the overall structure to obtain graphene thin film onto Si wafer after etching away the Ni-silicides. RGO was chemically prepared using graphite as a starting material which was oxidized and exfoliated using the improved Hummers method and then reduced with ascorbic acid to obtain RGO powder. RGO was mixed with PVA as a binder material to give RGO/PVA solution that was finally spincoated onto a Si wafer followed by heating the wafer to give RGO thin film. Samples were characterized using Raman, XRD and EDX analysis. The quality of the prepared films was qualified by a new proposed quality factor (Q) that is mainly dependent on Raman analysis and XRD calculations. The prepared samples showed comparable quality to their published counterparts. The electric conductivity of graphene and RGO samples was measured and compared with other published works. Graphene and RGO samples showed a comparable electrical conductivity value to similar reported counterparts. However, graphene thin film shows higher electric conductivity relative to RGO thin film which is in agreement with the proposed quality factor results. Generally, physical bottom-up approaches show higher product quality and conductivity compared to topdown methods due to lower structure defects. However, the complexity, high cost and limited scalability problems may limit the use of this technique. So, future studies could focus on optimizing bottom-up synthesis techniques to scale up the production of high-quality graphene through bottom-up methods by overcoming these complexities and limitations.

ACKNOWLEDGMENTS

The experimental work was supported by the Department of Chemical Engineering at the Military Technical College, Cytotoxicity Lab-Faculty of Nanotechnology for Postgraduate Studies-Cairo University and Zewail City of Science and Technology labs.

REFERENCES

- [1] S. Setiadji *et al.*, "Preparation of reduced Graphene Oxide (rGO) assisted by microwave irradiation and hydrothermal for reduction methods," *IOP Conference Series: Materials Science and Engineering*, vol. 434, p. 012079, 2018, doi: 10.1088/1757-899X/434/1/012079.
- [2] P. Tambe, "Synthesis and characterization of acid treated reduced graphene oxide," *Materials Today: Proceedings*, vol. 49, pp. 1294–1297, 2021, doi: 10.1016/j.matpr.2021.06.381.
- [3] M. Khaled, A. Zaki, and H. Shawkey, "Synthesis, characterization and qualification of graphene for electronic applications," *Journal of Engineering Science and Military Technologies*, vol. 8, no. 1, pp. 47–60, 2023, doi: 10.21608/ejmtc.2023.214102.1257.
- [4] S. C. Ray, D. K. Mishra, H. T. Wang, S. Bhattacharya (Mitra), and W. F. Pong, "Effects of electronic

- structure and magnetic performance at the surface/interface of r-GO and TiO_2 in r-GO/ TiO_2 composite thin films: X-ray absorption near-edge structure and x-ray photoelectron spectroscopy," *AIP advances*, vol. 12, no. 7, p. 075101, 2022, doi: 10.1063/5.0096305.
- [5] S. R. Khanna, M. G. Stanford, I. V. Vlassiouk, and P. D. Rack, "Combinatorial Cu-Ni Alloy Thin-Film Catalysts for Layer Number Control in Chemical Vapor-Deposited Graphene," *Nanomaterials*, vol. 12, no. 9, pp. 1553–1553, 2022, doi: 10.3390/nano12091553.
- [6] T. I. Milenov *et al.*, "Deposition of defected graphene on (001) Si substrates by thermal decomposition of acetone," *Superlattices and microstructures*, vol. 111, pp. 45–56, 2017, doi: 10.1016/j.spmi.2017.04.042.
- [7] Z. Wang *et al.*, "Synthesis of high-quality vertical graphene nanowalls on metal foams and their applications in EMI shielding," *Materials Today Communications*, vol. 33, p. 104608, 2022, doi: 10.1016/j.mtcomm.2022.104608.
- [8] N. Zebardastan *et al.*, "High quality epitaxial graphene on 4H-SiC by face-to-face growth in ultra-high vacuum," *Nanotechnology*, vol. 34, no. 10, pp. 105601–105601, 2022, doi: 10.1088/1361-6528/aca8b2.
- [9] X. Yang *et al.*, "The role of copper on the restoration of graphene oxide by chemical vapor deposition," *Materials Research Express*, vol. 8, no. 5, 2021, p. 055601. doi: 10.1088/2053-1591/abfb2a.
- [10] Y. Zhao *et al.*, "Study on Preparation and Properties of Ultrahigh Molecular Weight Polyethylene Composites Filled with Different Carbon Materials," *ACS Omega*, vol. 7, no. 6, pp. 5547–5557, 2022, doi: 10.1021/acsomega.1c07023.
- [11] J. J. Lander, H. E. Kern, and A. L. Beach, "Solubility and Diffusion Coefficient of Carbon in Nickel: Reaction Rates of Nickel-Carbon Alloys with Barium Oxide," *Journal of Applied Physics*, vol. 23, no. 12, pp. 1305–1309, 1952, doi: 10.1063/1.1702064.
- [12] Z.-Y. Juang *et al.*, "Synthesis of graphene on silicon carbide substrates at low temperature," *Carbon*, vol. 47, no. 8, pp. 2026–2031, 2009. doi: 10.1016/j.carbon.2009.03.051.
- [13] P. R. Kidambi *et al.*, "Observing Graphene Grow: Catalyst–Graphene Interactions during Scalable Graphene Growth on Polycrystalline Copper," *Nano Letters*, vol. 13, no. 10, pp. 4769–4778, 2013, doi: 10.1021/nl4023572.
- [14] J. Baek, J. Kim, J. Kim, B. Shin, and S. Jeon, "Growth of graphene on non-catalytic substrate by controlling the vapor pressure of catalytic nickel," *Carbon*, vol. 143, pp. 294–299, 2019, doi: 10.1016/j.carbon.2018.11.027.
- [15] J. Sun *et al.*, "Growth mechanism of graphene on platinum: Surface catalysis and carbon segregation," *Applied Physics Letters*, vol. 104, no. 15, 2014. doi: 10.1063/1.4871978.
- [16] M. Losurdo, M. M. Giangregorio, P. Capezzuto, and G. Bruno, "Graphene CVD growth on copper and nickel: role of hydrogen in kinetics and structure," *Physical Chemistry Chemical Physics*, vol. 13, no. 46, pp. 20836–20843, 2011, doi: 10.1039/c1cp22347j.

- [17] P. Macháč, T. Fidler, S. Cichoň, and L. Mišková, "Synthesis of graphene on SiC substrate via Nisilicidation reactions," *Thin Solid Films*, vol. 520, no. 16, pp. 5215–5218, 2012. doi: 10.1016/j.tsf.2012.03.105.
- [18] J. Prekodravac *et al.*, "The effect of annealing temperature and time on synthesis of graphene thin films by rapid thermal annealing," *Synthetic Metals*, vol. 209, pp. 461–467, 2015. doi: 10.1016/j.synthmet.2015.08.015.
- [19] K. N. Kudin, B. Ozbas, H. C. Schniepp, R. K. Prud'homme, I. A. Aksay, and R. Car, "Raman Spectra of Graphite Oxide and Functionalized Graphene Sheets," *Nano Letters*, vol. 8, no. 1, pp. 36–41, 2008. doi: 10.1021/nl071822y.
- [20] A. C. Ferrari and D. M. Basko, "Raman spectroscopy as a versatile tool for studying the properties of graphene," *Nature Nanotechnology*, vol. 8, no. 4, pp. 235–246, 2013, doi: 10.1038/nnano.2013.46.
- [21] M. Wall, "The Raman spectroscopy of graphene and the determination of layer thickness," *Thermo Scientific Application Note AN52252*, pp. 1–5, 2011.
- [22] M. Sahoo, R. P. Antony, T. Mathews, S. Dash, and A. K. Tyagi, "Raman studies of chemically and thermally reduced graphene oxide," *AIP Conference Proceedings*, vol. 1512, no. 1, 2013, doi: 10.1063/1.4791511.
- [23] A. Kaniyoor and S. Ramaprabhu, "A Raman spectroscopic investigation of graphite oxide derived graphene," *AIP Advances*, vol. 2, no. 3, p. 032183, 2012, doi: 10.1063/1.4756995.
- [24] N. E. Sorokina, M. A. Khaskov, V. V. Avdeev, and I. V. Nikol'skaya, "Reaction of Graphite with Sulfuric Acid in the Presence of KMnO₄," *Russian Journal of General Chemistry*, vol. 75, no. 2, pp. 162–168, 2005. doi: 10.1007/s11176-005-0191-4.
- [25] S. V. Tkachev, E. Y. Buslaeva, A. V. Naumkin, S. L. Kotova, I. V. Laure, and S. P. Gubin, "Reduced graphene oxide," *Inorganic Materials*, vol. 48, no. 8, pp. 796–802, 2012, doi: 10.1134/S0020168512080158.
- [26] Q. A. Khan, A. Shaur, T. A. Khan, Y. F. Joya, and M. S. Awan, "Characterization of reduced graphene oxide produced through a modified Hoffman method," *Cogent Chemistry*, vol. 3, no. 1, p. 1298980, 2017, doi: 10.1080/23312009.2017.1298980.
- [27] M. M. Lucchese *et al.*, "Quantifying ion-induced defects and Raman relaxation length in graphene," *Carbon*, vol. 48, no. 5, pp. 1592–1597, 2010, doi: 10.1016/j.carbon.2009.12.057.
- [28] V. Kumar, A. Kumar, M. Song, D.-J. Lee, S.-S. Han, and S.-S. Park, "Properties of silicone rubber-based composites reinforced with few-layer graphene and iron oxide or titanium dioxide," vol. 13, no. 10, p. 1550, 2021, doi: 10.3390/polym13101550.
- [29] Y. Hwangbo *et al.*, "Interlayer non-coupled optical properties for determining the number of layers in arbitrarily stacked multilayer graphenes," *Carbon*, vol. 77, pp. 454–461, 2014, doi: 10.1016/j.carbon.2014.05.050.
- [30] N. M. S. Hidayah *et al.*, "Comparison on graphite, graphene oxide and reduced graphene oxide:

- Synthesis and characterization," *AIP Conference Proceedings*, Vol. 1892, No. 1, p. 150002, 2017. doi: 10.1063/1.5005764.
- [31] R. Muzyka, S. Drewniak, T. Pustelny, M. Chrubasik, and G. Gryglewicz, "Characterization of Graphite Oxide and Reduced Graphene Oxide Obtained from Different Graphite Precursors and Oxidized by Different Methods using Raman Spectroscopy," *Materials*, vol. 11, no. 7, p. 1050, 2018. 10.3390/ma11071050.
- [32] A. N. Popova, "Crystallographic analysis of graphite by X-Ray diffraction," *Coke and Chemistry*, vol. 60, pp. 361–365, 2017. doi: 10.3103/S1068364X17090058.
- [33] S. Abdolhosseinzadeh, H. Asgharzadeh, and H. Seop Kim, "Fast and fully-scalable synthesis of reduced graphene oxide," *Scientific Reports*, vol. 5, no. 1, p. 10160, 2015. doi: 10.1038/srep10160.
- [34] B. Huang, Q. Wang, Y. Li, M. Zhang, and X. Wei, "Preparation and characterisation of graphene," *Materials Research Innovations*, vol. 19, no. sup9, pp. S9-344–S9-350, 2015, doi: 10.1179/1432891715Z.0000000002010.
- [35] K. M. Kar, *Handbook of Fly Ash*, 1st ed. Elsevier, 2021. doi: 10.1016/C2018-0-01655-2.
- [36] A. Bhaumik *et al.*, "Reduced Graphene Oxide Thin Films with Very Large Charge Carrier Mobility Using Pulsed Laser Deposition," *Journal of Material Science & Engineering*, vol. 6, no. 4, 2017, doi: 10.4172/2169-0022.1000364.
- [37] W. Ouyang *et al.*, "Exploring the active sites of nitrogen-doped graphene as catalysts for the oxygen reduction reaction," *International Journal of Hydrogen Energy*, vol. 39, no. 28, pp. 15996–16005, 2014, doi: 10.1016/j.ijhydene.2014.01.045.
- [38] D. Selvakumar, A. Alsalme, A. Alswieleh, and R. Jayavel, "Freestanding flexible nitrogen doped-reduced graphene oxide film as an efficient electrode material for solid-state supercapacitors," *Journal of Alloys and Compounds*, vol. 723, pp. 995–1000, 2017, doi: 10.1016/j.jallcom.2017.06.333.
- [39] N. Akbar *et al.*, "Biosynthesis of Graphene and Investigation of Antibacterial Activity of Graphene-parthenium hysterophorous Nanocomposite," *Brazilian Archives of Biology and Technology* (Impresso), vol. 64, p. e21210180, 2021, doi: 10.1590/1678-4324-2021210180.
- [40] F. T. Thema *et al.*, "Synthesis and Characterization of Graphene Thin Films by Chemical Reduction of Exfoliated and Intercalated Graphite Oxide," *Journal of Chemistry*, vol. 2013, pp. 1–6, 2013, doi: 10.1155/2013/150536.
- [41] H. Guo *et al.*, "Epitaxial growth and electrical performance of graphene/3C–SiC films by laser CVD," *Journal of alloys and compounds*, vol. 826, p. 154198, 2020, doi: 10.1016/j.jallcom.2020.154198.
- [42] S. Soni, P. Sathe, S. K. Sarkar, A. Kushwaha, and D. Gupta, "Inkjet-printed sub-zero temperature sensor for real-time monitoring of cold environments," *International journal of biological macromolecules*, vol. 258, p. 128774, 2024, doi: 10.1016/j.ijbiomac. 2023.128774.

- [43] E. Jaafar, M. Kashif, S. K. Sahari, and Z. Ngaini, "Study on Morphological, Optical and Electrical Properties of Graphene Oxide (GO) and Reduced Graphene Oxide (rGO)," *Materials Science Forum*, vol. 917, pp. 112–116, 2018, doi: 10.4028/www.scientific.net/MSF. 917.112.
- [44] S. A. Rag, M. Selvakumar, S. Bhat, S. Chidangil, and S. De, "Synthesis and Characterization of Reduced Graphene Oxide for Supercapacitor Application with a Biodegradable Electrolyte," *Journal of Electronic Materials*, vol. 49, no. 2, pp. 985–994, 2019, doi: 10.1007/s11664-019-07853-9.